

High-frequency performance of graphene field effect transistors with saturating IV-characteristics

Inanc Meric¹, Cory R. Dean^{1,2}, Shu-Jen Han³, Lei Wang², Keith A. Jenkins³, James Hone², and K. L. Shepard¹

¹Department of Electrical Engineering, ²Department of Mechanical Engineering, Columbia University, New York, NY, 10027

³IBM T.J. Watson Research Center, Yorktown Heights, NY 10598

Tel: (646) 205-0438, Fax: (212) 932-9421, Email: shepard@ee.columbia.edu

Abstract

High-frequency performance of graphene field-effect transistors (GFETs) with boron-nitride gate dielectrics is investigated. Devices show saturating IV characteristics and f_{max} values as high as 34 GHz at 600-nm channel length. Bias dependence of f_T and f_{max} and the effect of the ambipolar channel on transconductance and output resistance are also examined.

Introduction

Interest remains high in the potential use of graphene as a field-effect transistor (FET) channel replacement material [1, 2]. The focus is primarily on analog and RF applications of graphene FETs (GFETs) because of the limited on-current-to-off-current ratios achievable with this zero-bandgap material. Within the last few years, the RF performance of GFETs, as determined by the device current-gain cut-off frequency (f_T), has gone from 15 GHz [3] for 500-nm-length devices in the

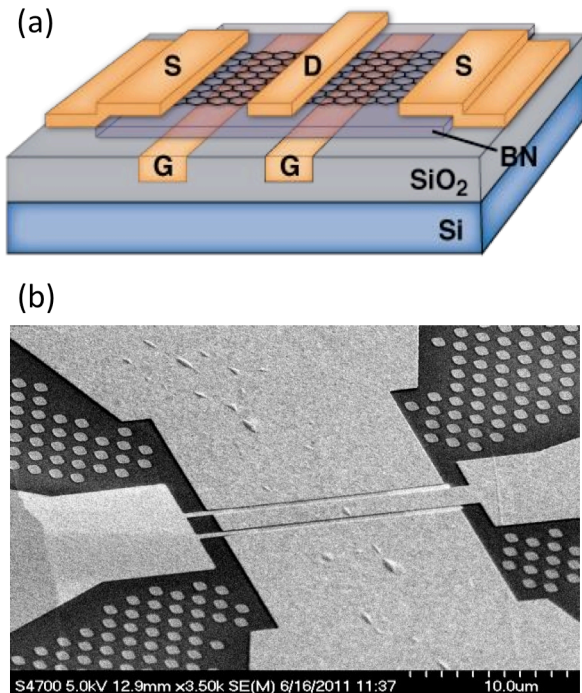


Figure 1. GFET device structure. (a) Schematic illustration of the back-gated GFET device. (b) SEM micrograph of a completed structure.

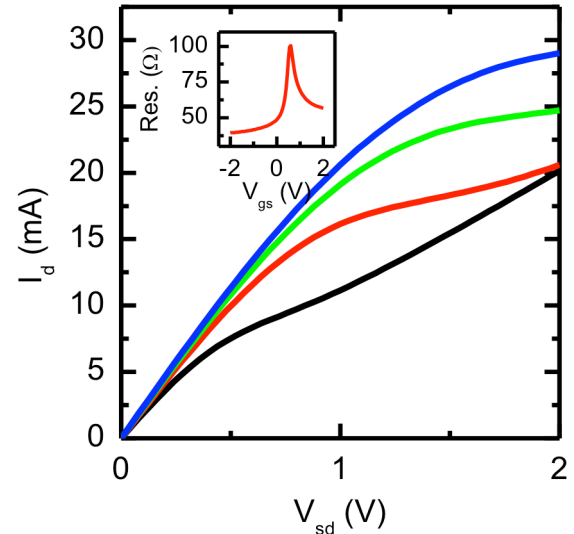


Figure 2. IV characteristics. I_D as a function of V_{sd} for V_{gs} from 0V to -1.5V in 0.5V steps. Inset: Resistance in linear transport region as a function of V_{gs} .

first measurements to 155 GHz at 40-nm channel lengths in the most recent reports [4].

RF measurements have generally been reported for top-gated

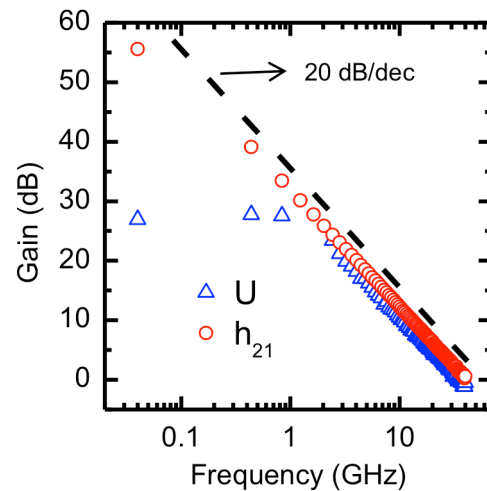


Figure 3. High-frequency device characteristics. h_{21} and unilaterial power gain (U) as a function of frequency after deembedding, yielding $f_T = 44$ GHz and $f_{max} = 34$ GHz.

device structures whose current-voltage characteristics do not show strong current saturation due to relatively poor gate-oxide interfaces or weak gate coupling. As a result, device output conductance is high, power gain is limited, and the maximum oscillation frequency (f_{max}) is typically only one-tenth of f_T . In this work, by exploiting high-quality boron-nitride dielectrics, we instead find f_{max}/f_T ratios as high as 0.86 and f_{max} values as high as 34 GHz for a 600-nm-length device, the highest value reported so far for GFETs. We further investigate the bias dependence of both f_T and f_{max} and compare our results with small-signal models of our device structures.

Device Fabrication

Hexagonal boron nitride (h-BN) has been previously found to be an outstanding gate dielectric for GFETs, yielding

interfaces nearly free of trapped charge and maintaining high mobility and carrier velocities in the graphene channel [5, 6]. The GFETs characterized here are created with a back gate as shown in Fig. 1a. A split-gate layout is employed, where tungsten metal gates are initially patterned into a 1- μm SiO₂ layer using a Damascene-like process, followed by a chemical-mechanical polishing (CMP) step to ensure a flat surface and expose the gate metal surface. h-BN (10-nm thick) is mechanically transferred to form the gate dielectric, followed by the mechanical transfer of the graphene channel (single layer). GFET fabrication ends with e-beam patterning of source and drain contacts with approximately 50-nm gate-to-source and gate-to-drain spacings as shown in Fig. 1a. An SEM micrograph of a completed device is shown in Fig. 1b.

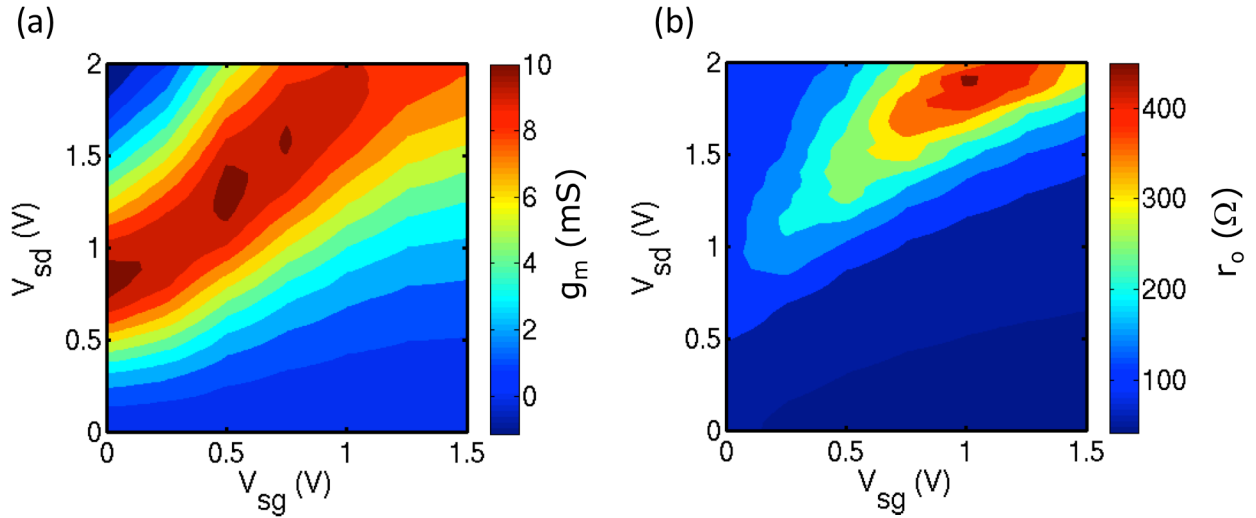


Figure 4. Bias-dependence of small-signal parameters. (a) Transconductance and (b) output resistance.

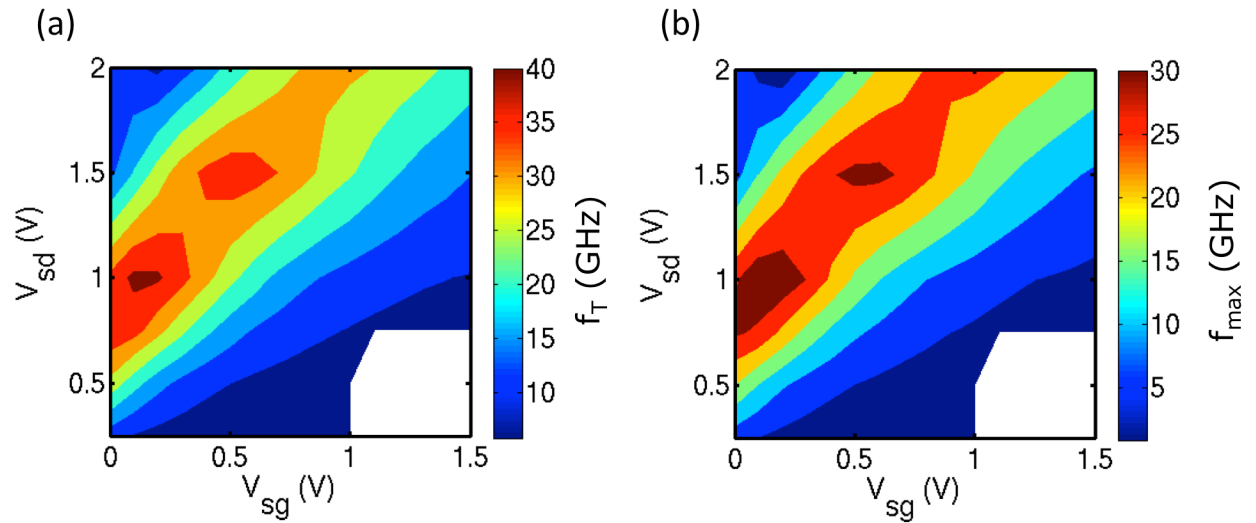
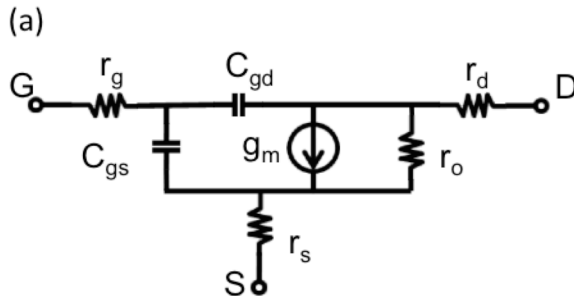


Figure 5. Bias dependence of high-frequency figures-of-merit. (a) f_T and (b) f_{max} .

DC Measurements

Fig. 2 shows the DC current-voltage (IV) characteristic of a representative GFET device with an effective width of approximately 38 μm and channel length of 0.6 μm . The inset of Fig. 2 shows the accompanying source-drain resistance in the triode region at $V_{sd} = 10$ mV, from which the contact resistance and low-field mobility can be extracted. The total contact resistance (including both source and drain) is approximately 25 Ω , or 950 $\Omega\text{-}\mu\text{m}$ when normalized to contact width. (Contact resistance is inversely proportional to contact width.) The low-field mobility is 3,300 $\text{cm}^2/\text{V sec}$. The charge neutrality point (V_o), the gate-to-source voltage at which the maximum low-field triode resistance is achieved, is 0.6 V. IV characteristics are plotted for gate voltages (V_{sg}) from 0 to -1.5V, demonstrating both saturating current characteristics for the unipolar hole channel and the “kink” associated with the transition to the ambipolar hole-electron



(b)

g_m	19 mS	r_s, r_d	12.5 Ω
r_o	98 Ω	C_{gd}	17 fF
r_g	19 Ω	C_{gs}	34 fF

(c)

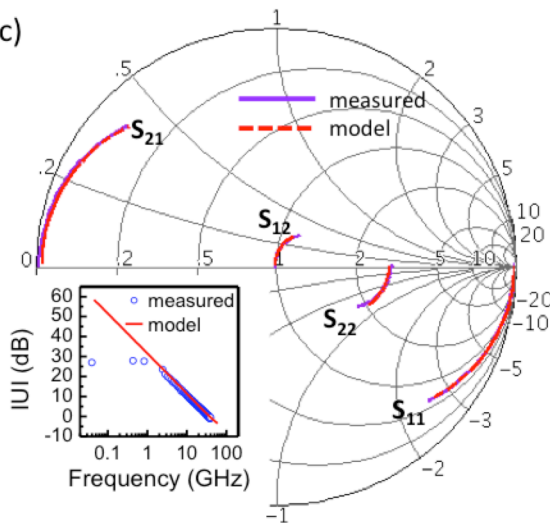


Figure 6. Small-signal modeling. (a) Small-signal equivalent circuit for a representative 0.6- μm transistors; (b) parameter values used in the model; and (c) measured S-parameters along with the results of the model. Inset: Unilateral gain of both measured and modeled device.

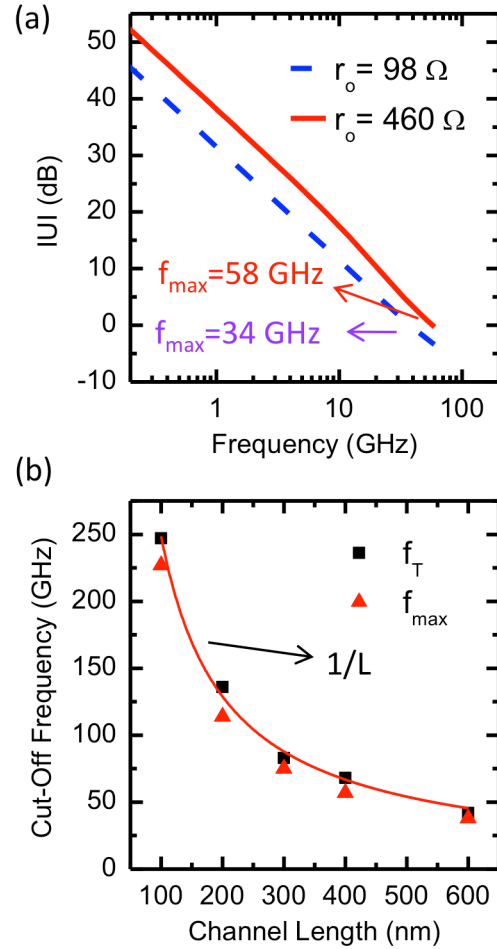


Figure 7. Improvements possible with device optimization. (a) U calculated from the model with parameter values of Fig. 6b (dashed blue) and with output resistance set to highest measured value (red). (b) Predicted high-frequency performance at different channel lengths.

channel. Fig. 4 gives the transconductance (g_m) and output resistance (r_o) as a function of bias; both are strongly influenced by the kink behavior in the IV characteristic. The peak g_m of 10.5 mS and peak r_o of 460 Ω occur at different bias points. The devices show no hysteresis and unchanged characteristics after repeated measurements.

High-Frequency Measurements

Device S-parameters are measured to 40 GHz. Standard “open-short” de-embedding methods are employed. In Fig. 3, current-gain (h_{21}) and unilateral power gain (U) are plotted at the bias point of peak g_m , yielding f_T and f_{max} of 44 GHz and 34 GHz, respectively. (Without de-embedding f_T and f_{max} are 24 GHz and 17 GHz, respectively.) Fig. 5 shows f_T and f_{max} as a function of bias; the peak high-frequency response closely matches the peak transconductance of the device.

The small-signal model of Fig. 6a is used to model the high-frequency behavior of the GFETs. The measured S-

parameters are shown in Fig. 6c, showing good agreement with the results of the small signal model with the parameters given in Fig. 6b. These small-signal values are in good agreement with values derived from the IV characteristics. The g_m here is the intrinsic value, exclusive of contact resistance, in good agreement with our previous results of approximately 0.5 mS/ μm [6].

The model derived from this representative 0.6- μm device can be used to further understand device optimization and scaling. Fig. 7a shows how the f_{max} performance could be improved to 58 GHz for this same channel length if the V_o of the device could be adjusted (through a secondary gate or channel doping) to align peak g_m and r_o . The model is also used to estimate the performance at shorter channel lengths by scaling gate capacitance while keeping other small-signal parameters constant as shown in Fig. 7b. f_{max} values close to 250 GHz are possible at 100 nm channel length. Higher frequency performance will require significant improvements in device parasitics, most notably the contact resistance.

Acknowledgments

The authors would like to thank K. Watanabe and T. Taniguchi for supplying h-BN crystals. The authors acknowledge the support of the C2S2 Focus Center, one of six research centers funded under the Focus Center Research Program (FCRP), a Semiconductor Research Corporation

entity, and DARPA under contract FA8650-08-C-7838 through the CERA program, and by the AFOSR MURI Program on new graphene materials technology, FA9550-09-1-0705.

References

- [1] F. Schwierz, "Graphene transistors," *Nature Nanotechnology*, vol. 5, pp. 487-96, Jul 1 2010.
- [2] P. Avouris, "Graphene: Electronic and Photonic Properties and Devices," *Nano Letters*, pp. 4285-4294, Sep 29 2010.
- [3] I. Meric, N. Baklitskaya, P. Kim, and K. L. Shepard, "RF performance of top-gated, zero-bandgap graphene field-effect transistors," in *Electron Devices Meeting, 2008. IEDM 2008. IEEE International*, San Francisco, CA, USA, 2008.
- [4] Y. Wu, Y.-M. Lin, A. A. Bol, K. A. Jenkins, F. Xia, D. B. Farmer, Y. Zhu, and P. Avouris, "High-frequency, scaled graphene transistors on diamond-like carbon," *Nature*, vol. 472, pp. 74-8, Apr 7 2011.
- [5] C. R. Dean, A. F. Young, I. Meric, C. Lee, L. Wang, S. Sorgenfrei, K. Watanabe, T. Taniguchi, P. Kim, K. L. Shepard, and J. Hone, "Boron nitride substrates for high-quality graphene electronics," *Nature Nanotechnology*, vol. 5, pp. 722-726, Aug 22 2010.
- [6] I. Meric, C. Dean, A. Young, J. Hone, P. Kim, and K. L. Shepard, "Graphene field-effect transistors based on boron nitride gate dielectrics," presented at the Electron Devices Meeting (IEDM), 2010 IEEE International, 2010. , pp. 23.2.1-23.2.4.